The Astrophysical Journal, 669:1085–1097, 2007 November 10

GRAIN ALIGNMENT AND POLARIZED EMISSION FROM MAGNETIZED T TAURI DISKS

Jungyeon Cho
Department of Astronomy and Space Science, Chungnam National University, Daejeon, South Korea; jcho@cnu.ac.kr

and

A. Lazarian
Astronomy Department, University of Wisconsin, Madison, WI 53706; lazarian@astro.wisc.edu
Received 2006 October 4; accepted 2007 July 21

ABSTRACT

The structure of magnetic fields within protostellar disks may be studied via polarimetry provided that grains are aligned with respect to the magnetic field within the disks. We explore the alignment of dust grains by radiative torque in T Tauri disks and provide predictions for polarized emission for disks viewed at different wavelengths and viewing angles. We show that the alignment is especially efficient in the outer parts of the disks. In the presence of a magnetic field, these aligned grains produce polarized emission in infrared wavelengths. We consider a simple disk model and provide predictions for polarization that are available to the present-day instruments that do not resolve the disks and will be available to future instruments that will resolve the disks. We find that the polarized emission drops for wavelengths shorter than $\sim$10 μm. Between $\sim$10 and $\sim$100 μm, the polarized emission is dominated by the emission from the surface layer, and the degree of polarization can be as large as $\sim$10% for unresolved disks. We find that the degree of polarization at these wavelengths is very sensitive to the size distribution of dust grains in the disk surface layer, which should allow for the testing of the predicted grain-size distributions. The degree of polarization in the far-infrared/submillimeter wavelengths is sensitive to the size distribution of dust grains in the disk interior. When we take a Mathis-Rumpl-Nordsieck–type distribution with maximum grain size of 500–1000 μm, the degree of polarization is around the 2%–3% level at wavelengths larger than $\sim$100 μm. Our study indicates that multifrequency infrared polarimetric studies of protostellar disks can provide good insights into the details of their magnetic structure.

Subject headings: accretion, accretion disks — circumstellar matter — dust, extinction — polarization — stars: pre–main-sequence

1. INTRODUCTION

Magnetic fields play important roles in star formation as well as formation and evolution of protostellar disks. Magnetic pressure can provide extra support to the disks and magnetic fields can promote the removal of angular momentum from disks (see Velikov 1959; Chandrasekhar 1961; Balbus & Hawley 1991). However, there are many uncertainties for the structure and effects of the magnetic field in protostellar disks.

Infrared (IR) polarimetry may be an important tool for investigating magnetic field structure in protostellar disks, provided that the grains are aligned in the disks with respect to the magnetic field. Since the grain emissivity is larger for the long axis of a grain, emitted radiation has a polarization vector parallel to the grain's long axis. If grains are aligned with their long axes perpendicular to the magnetic field, the resulting grain emission has polarization directed perpendicular to the magnetic field. Therefore, by measuring the direction of polarization of IR emission from dust grains one can infer the direction of magnetic field. The key question, thus, is whether grain alignment is efficient in protostellar disks.

The notion that the grains can be aligned with respect to the magnetic field can be traced back to the discovery of starlight polarization by Hall (1949) and Hiltner (1949), which arises from interstellar grains. Historically, the theory of the grain alignment was primarily developed to explain the interstellar polarization, but grain alignment is a much more widespread phenomenon (see Lazarian 2007 for a review). Among the alignment mechanisms that are related to radiative torques (RTs) looks the most promising. We invoke it for our calculations below.

The RTs make use of interaction of radiation with a grain to spin the grain up. The RT alignment was first discussed by Dolginov (1972) and Dolginov & Mytrophanov (1976). However, quantitative studies were done only in the 1990s. In their pioneering work, Draine & Weingartner (1996 [hereafter DW96], 1997) demonstrated the efficiency of the RT alignment for a few arbitrarily chosen irregular grains using numerical simulations. This work identified RTs as potentially the major agent for interstellar grain alignment. Cho & Lazarian (2005, hereafter CL05) demonstrated the rapid increase of radiative torque efficiency and showed that radiative alignment can naturally explain the decrease of the degree of polarization near the centers of prestellar cores. Large grains are known to be present in protostellar disk environments and this makes the RT alignment promising.

The effect of RTs is two-fold. They can spin up grains, and they can drive the alignment. While the details of the second process are a subject of intensive research (see Weingartner & Draine 2003; Lazarian & Hoang 2007; Hoang & Lazarian 2007), for our estimates we use the RT spin-up efficiency to evaluate the efficiency of grain alignment. As grains of different temperatures are present in protostellar disks, the differential alignment of grains at different optical depths is expected to show itself through variations of polarization at different wavelengths.

Protostellar disks are often detected through far-IR excess. Dust grains in the protostellar disks are the main cause of the IR excess; dust grains absorb stellar radiation and re-emit at IR wavelengths. The spectral energy distribution (SED) of the emitted light gives valuable information about the disk structure. A recently proposed hydrostatic radiative-equilibrium passive-disk model (Chiang & Goldreich 1997; Chiang et al. 2001; hereafter CG97 and C01,

respectively) fits observed SEDs from T Tauri stars very well and seems to be one of the most promising models. Here, passive disk means that the active accretion effect, which might be very important in the immediate vicinity of the central star, is not included in the model. In this paper we use the model from C01.

Polarization arising from disks is of great interest and importance. Recently, Aitken et al. (2002) studied polarization that can arise from magnetized accretion disks. They considered a single grain component consisting of the 0.6 μm silicate and assumed that grains were partially aligned with $R = 0.25$, where $R = \langle 3\cos^2\beta - 1\rangle/2$ is the Rayleigh reduction factor (Greenberg 1968). Here, β is the precession angle between the grain spin axis and the magnetic field, and the angle brackets denote average (see Aitken et al. 2002 for details). In this paper we use both a theoretically motivated model of grain alignment and a more sophisticated model of the accretion disk.

Note that challenges of observing polarization in mid-IR to far-IR (FIR) wavelengths have been dealt with successfully recently. For instance, Tamura et al. (1999) first detected polarized emission from T Tauri stars, which are low-mass protostars. As technology develops, the future of polarimetric IR and submillimeter emission studies looks very promising. In this paper we try to theoretically predict polarized emission from T Tauri disks at different wavelengths and for different inclinations of the disks.

We calculate grain alignment by radiative torque using a T Tauri disk model from C01, and we predict polarized mid-IR/FIR/submillimeter emission. In § 2 we discuss grain alignment in T Tauri disks. In § 3 we give theoretical estimates for the degree of polarization. In § 4 we calculate the SED of *maximally* polarized emission, which will be useful only when we spatially resolve disks. In § 5 we discuss the effect of inclination angle. In § 6 we discuss observational implications. We give a summary in § 7.

2. GRAIN ALIGNMENT IN PROTOSTELLAR DISKS

2.1. *The Disk Model Used for This Study*

We assume that the magnetic field is regular and toroidal (i.e., *azimuthal*). We use a T Tauri disk model from C01. Figure 1 schematically shows the model. The disk is in hydrostatic and radiative equilibrium (see also CG97) and shows flaring. According to CG97, the flaring of the disk is essential for a correct description of the SED. They considered a two-layered disk model. Dust grains in the surface layer are heated directly by the radiation from the central star and emit their heat more or less isotropically. Half of the dust's thermal emission immediately escapes, and the other half enters into disk interior and heats dusts and gas there. Both CG97 and C01 assumed that the disk interior is isothermal.

In both CG97 and C01 the disk surface layer is hotter than the disk interior. Thus, roughly speaking, the surface layer dominates in mid-IR wavelengths and the disk interior dominates in FIR/submillimeter wavelengths. The disk surface layer is both optically and physically thin.

The major difference between CG97 and C01 is the treatment of the dust grain-size distribution. CG97 assumed that all grains have a fixed size of 0.1 μm, while C01 assumes an MRN distribution (Mathis et al. 1977) with maximum grain size of $a_{\max,i} = 1000$ μm in the disk interior and $a_{\max,s} = 1$ μm in the disk surface layer.

In our calculations, we use a grain model similar to that in C01. We use an MRN-type power-law distribution of grain radii a between $a_{\min}$ (0.01 μm for both disk interior and surface layer) and $a_{\max}$ (1000 μm for disk interior and 1 μm for disk surface layer) with a power index of -3.5: $dN \propto a^{-3.5}da$. As in C01, we assume that grain composition varies with distance from the central star in both the disk interior and the surface layer. We assume that grains in the surface layer are made of silicate only when the distance r is less than 6 AU and silicate covered with water ice when $r > 6$ AU. We do not use iron grains for the immediate vicinity of the star. We assume that grains in the disk interior are made of silicate when $r < 0.8$ AU and ice-silicate for $r > 0.8$ AU. The fractional thickness of the water ice mantle, $\Delta a/a$, is set to 0.4 for both the disk surface and the disk interior. Unlike C01, we use the refractive index of astronomical silicate (Draine & Lee 1984; Draine 1985; Laor & Draine 1993; see also Weingartner & Draine 2001). We take optical constants of pure water ice from a NASA Web site.[1]

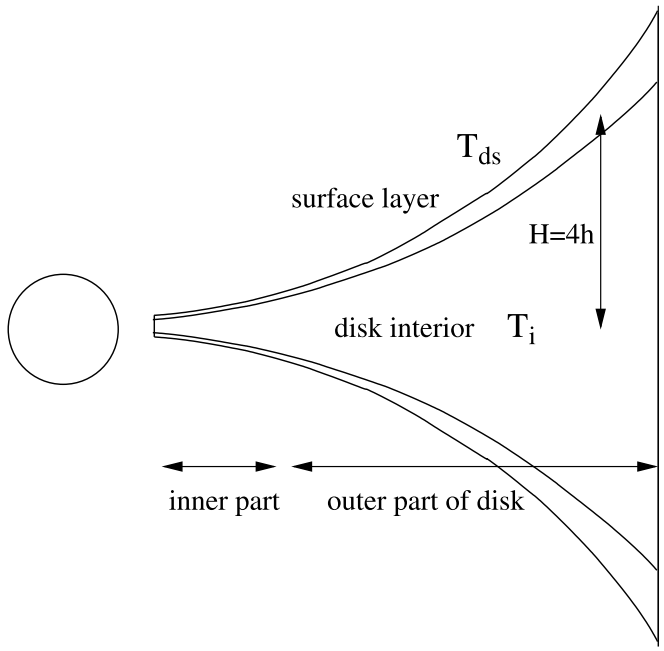

FIG. 1.—Schematic view of the disk model (see C01). The surface layer is hotter and heated by the star light. The disk interior is heated by reprocessed light from the surface layers. We assume that the disk height H is 4 times the disk scale height h.

The column density of the disk is $\Sigma_0 r_{\rm AU}^{-3/2}$, with $\Sigma_0 = 1000$ g cm^{-2}, where $r_{\rm AU}$ is distance measured in astronomical units. The disk is geometrically flared, and the height of the disk surface is set to 4 times the disk scale height h. The disk inner radius is $2R_*$, and the outer radius is 100 AU. The central star has a radius of $R_* = 2.5$ $R_\odot$ and a temperature of $T_* = 4000$ K. The temperature profile, flaring of the disk, and other details of the disk model are described in C01.

2.2. *Radiative Torque for Large Grains*

For most of the ISM problems, dust grains are usually smaller than the wavelengths of interest. However, this is no longer true in T Tauri disks, because we are dealing with grains as large as $\sim$1000 μm. To understand grain alignment in T Tauri disks, we need to know radiative torque for large grains.

In this study, we do not directly calculate radiative torque for large grains. Instead, we use a simple scaling relation to model radiative torque for large grains.

In CL05, we used the DDSCAT software package (Draine & Flatau 1994, 2004; Draine & Weingartner 1996) to calculate radiative torque on grain particles and showed the relation between λQ_Γ and λ/a for grains with radii between 0.1 and 3.2 μm.

[1] Available at ftp://climate1.gsfc.nasa.gov/wiscombe.

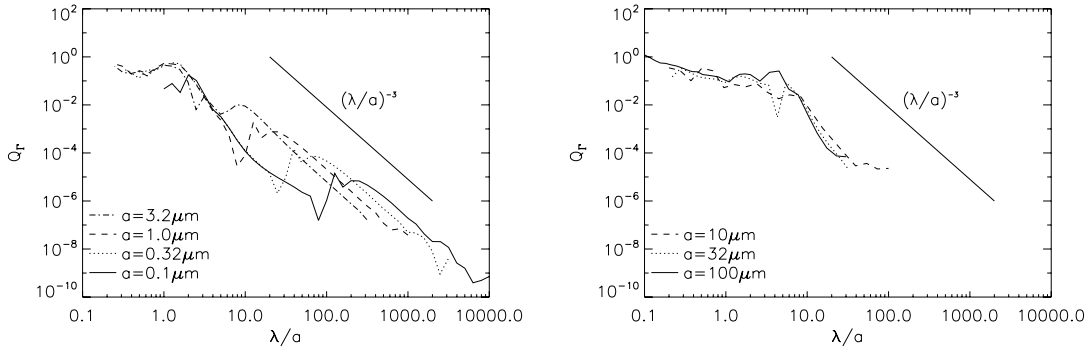

FIG. 2.—Behavior of torque. Torque is $\sim O(1)$ when $\lambda \sim a$, where a is the grain size. Roughly speaking, torque $\propto (\lambda/a)^{-3}$. *Left*: Results for small grains. Data from CL05. *Right*: Results for large grains. Data from Lazarian & Hoang (2007).

Here Q_Γ is the radiative torque efficiency. Figure 2, obtained by reprocessing the earlier relation, shows that the radiative torque

$$Q_\Gamma = \begin{cases} \sim O(1), & \text{if } \lambda \sim a, \\ \sim (\lambda/a)^{-3}, & \text{if } \lambda > a, \end{cases} \tag{1}$$

where a is the grain size and λ is the wavelength of the incident radiation. Note that the radiative torque peaks near $\lambda \sim a$ and that its value is of order unity there. A more general study on this issue is provided in Lazarian & Hoang (2007). This allows us to assume that the relation holds true for both small and large grains.

2.3. *Rotation Rate of Dust Grains by Radiative Torque*

To obtain grain rotational velocity one needs to calculate the balance between the excitation of rotation, driven by different processes, and the damping of rotational motions (see Draine & Lazarian 1998). Below we calculate the rotational rates of a grain driven by radiative torques and subjected to gaseous damping. Note that according to Lazarian & Hoang (2007), the obtained rates will not be the actual rotational rates of a grain that is free to get aligned under the influence of the anisotropic radiation. In fact, most of the grains will be driven to low-J attractor points and will rotate thermally or even subthermally. However, being driven by anisotropic radiation, grains get aligned and it was argued in Lazarian (2007) that the parameterization of the radiative torques in terms of the maximal achievable angular velocity is a valid one. Incidentally, this was also the parameterization that we used in CL05 and in the subsequent paper by Bethell et al. (2007).

After some modifications, equation (67) in DW96 reads

$$\left(\frac{\omega_{\rm rad}}{\omega_T}\right)^2 = 4.72\times10^9\,\frac{\alpha_1}{\delta^2}\,\rho_3 a_{-5}\left(\frac{u_{\rm rad}}{n_{\rm H}kT}\right)^2 \times\left(\frac{\lambda}{1\ \mu{\rm m}}\right)^2 Q_\Gamma^2\left(\frac{\tau_{\rm drag}}{\tau_{\rm drag,gas}}\right)^2, \tag{2}$$

where $Q_\Gamma = \boldsymbol{Q}_\Gamma\cdot\hat{\boldsymbol{a}}_1$ and $\hat{\boldsymbol{a}}_1$ is the principal axis with largest moment of inertia, $n_{\rm H}$ is the hydrogen number density, $u_{\rm rad}$ is the energy density of the radiation field, $\delta \approx 2$, $\alpha_1 \approx 1.745$, $\rho_3 = \rho/3$ g cm^{-3}, $a_5 = a/10^{-5}$ cm, and ω_T is the thermal angular frequency, which is the rate at which the rotational kinetic energy of a grain is equal to $kT/2$. The timescales $\tau_{\rm drag,gas}$ and $\tau_{\rm drag,em}$ are the damping time for gas drag and for electromagnetic emission, respectively, and they satisfy the relation $\tau_{\rm drag}^{-1} = \tau_{\rm drag,em}^{-1} + \tau_{\rm drag,gas}^{-1}$ (see Draine & Weingartner 1996 for details). As we discussed in § 2.2, Q_Γ is of order of unity when $\lambda \sim a$ and declines as (λ/a) increases. From this observation, we can write

$$\left(\frac{\omega_{\rm rad}}{\omega_T}\right)^2 \approx \left(\frac{\omega_{\rm rad}}{\omega_T}\right)^2_{\lambda\sim a}\left(\frac{Q_{\Gamma,\lambda\sim a}}{Q_{\Gamma,\lambda}}\right)^2 \approx \left(\frac{\omega_{\rm rad}}{\omega_T}\right)^2_{\lambda\sim a}\left(\frac{\lambda}{a}\right)^{-6} \tag{3}$$

for $\lambda > a$, where

$$\left(\frac{\omega_{\rm rad}}{\omega_T}\right)^2_{\lambda\sim a} \approx 4.72\times10^9\,\frac{\alpha_1}{\delta^2}\,\rho_3 a_{-5}\left(\frac{u_{\rm rad}}{n_{\rm H}kT}\right)^2 \times\left(\frac{\lambda}{1\ \mu{\rm m}}\right)^2\left(\frac{\tau_{\rm drag}}{\tau_{\rm drag,gas}}\right)^2. \tag{4}$$

2.4. *Minimum and Maximum Aligned Grain Size*

As in DW96, we assume that grains are aligned when $(\omega_{\rm rad}/\omega_T)^2 > 10$. Suppose that a monochromatic radiation field illuminates dust grains and that $(\omega_{\rm rad}/\omega_T)^2 > 10$ for $\lambda \sim a$. According to equation (2), the ratio $(\omega_{\rm rad}/\omega_T)^2$ decreases as a decreases and the ratio will drop below $\sim$10. Applying equation (3), we can easily find the minimum aligned grain size,

$$a_{\rm lower} \sim \lambda\left[\frac{10}{(\omega_{\rm rad}/\omega_T)^2_{\lambda\sim a}}\right]^{1/6}. \tag{5}$$

Then, how can we find the maximum aligned grain size? In other words, are all grains with $a > \lambda$ aligned? In order to answer this question, we need to consider the behavior of torque Q_Γ for the limit $a \gg \lambda$. Note that when $\lambda \sim a$, $Q_\Gamma \sim O(1)$. Then what happens when $a \gg \lambda$? In principle, we can calculate Q_Γ using numerical simulations. However, this is still infeasible because enormous computational power is required. Therefore, we can only conjecture what will happen for $a \gg \lambda$.

If one adopts the reasoning for the origin of RT in Dolginov & Mytrophanov (1976), one might expect that Q_Γ drops due to incoherent contributions. Theoretical considerations in Lazarian & Hoang (2007) show that this may not be true. While to be conservative we adopt a rule of thumb that Q_Γ may begin to decline when $a \geq 10\lambda$, we see below that this assumption does not alter our results in any appreciable way.[2]

[2] Note that here λ is the wavelength at which radiation is strongest. For most cases, $\lambda = \lambda_{\rm max,Wien} \propto 1/T$ when the radiation field is a blackbody radiation, where $\lambda_{\rm max,Wien}$ is the $\lambda_{\rm max}$ from Wien's law.

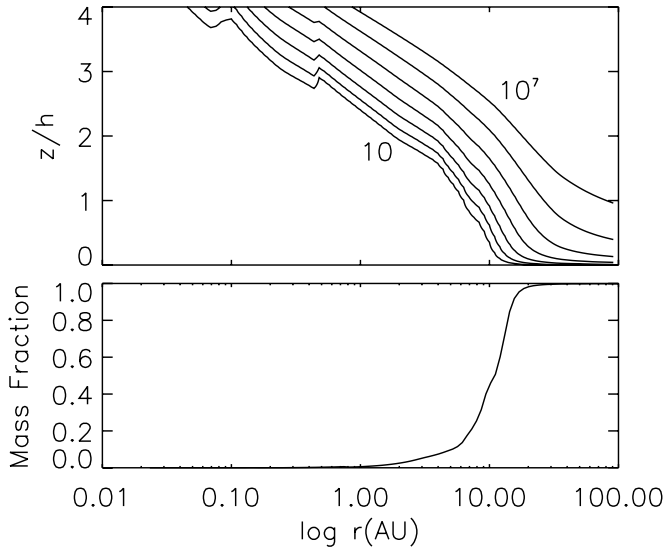

FIG. 3.—Grain alignment in disk interior. *Top*: Contours show the ratio $(\omega_{\rm rad}/\omega_T)^2_{\lambda\sim a}$. Note that the disk vertical height is shown in units of the disk scale height h. We assume that grains are aligned when $(\omega_{\rm rad}/\omega_T)^2 > 10$. *Bottom*: Fraction of grains that satisfy $(\omega_{\rm rad}/\omega_T)^2_{\lambda\sim a} > 10$ as a function of disk radius. After $r > 10$ AU, almost 100% of grains satisfy the inequality.

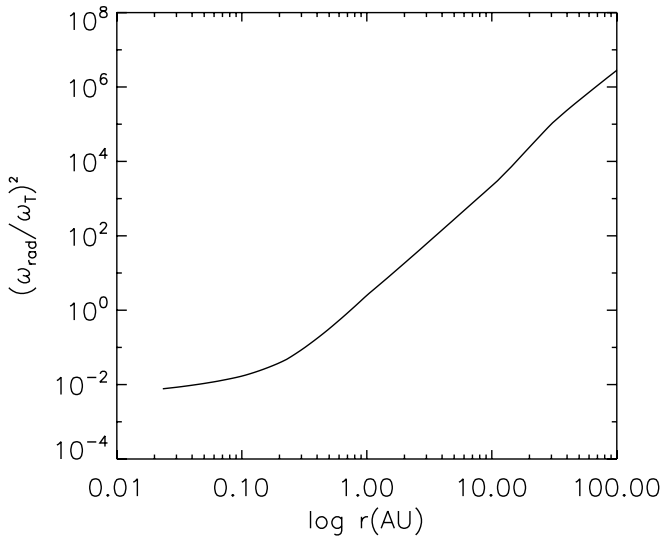

FIG. 4.—Grain alignment in surface layer. The ratio $(\omega_{\rm rad}/\omega_T)^2_{\lambda\sim a}$ exceeds 10 when $r \geq 1$ AU, which means that some grains in the surface layer are aligned when $r \geq 1$ AU.

We also need to consider many different timescales: the precession timescale, the timescale for the alignment of angular momentum and $\hat{\boldsymbol{a}}_1$, etc. Fortunately, however, the exact knowledge on the maximum aligned grains size is not so important for our current study (see § 2.5).

2.5. *Grain Alignment in Disks*

We use equation (1) instead of the DDSCAT software package to obtain RT (Q_Γ) on grain particles in the T tauri disk described in § 2. We take a conservative value of Q_Γ at $\lambda \sim a$: $Q_\Gamma \sim 0.1$ at $\lambda \sim a$. Apart from Q_Γ, we also need to know $u_{\rm rad}$ and $n_{\rm H}$ to get the $(\omega_{\rm rad}/\omega_T)^2_{\lambda\sim a}$ ratio (see eq. [4]). We directly calculate $u_{\rm rad}$ and $n_{\rm H}$ using the disk model in C01. We assume that $\tau_{\rm drag} \sim \tau_{\rm drag,gas}$.

In the disk interior, there are two kinds of radiation fields: one from the surface layer and the other from the disk interior itself. We assume that both radiation fluxes direct only along the disk vertical axis (i.e., "z"-axis). As in CG97, we assume that half of the stellar radiation flux that reaches the disk surface enters the disk interior. The radiation flux from the star is $\sim(\alpha/2)(R_*/r)^2\sigma_{\rm B}T_*^4$, where α is the grazing angle at which the starlight strikes the disk, R_* is the stellar radius, T_* is the stellar temperature, and $\sigma_{\rm B}$ is the Stephan-Boltzmann constant (CG97). We assume that the radiation flux from the surface layer has a narrow spectrum around the wavelength of $\sim 3000/T_{ds}$ μm, where T_{ds} is the grain temperature in the surface layer (see C01 for a graph for T_{ds}). The magnitude of the flux from the surface at a given height is less than the half of the incident stellar flux because the flux from the surface is attenuated by dust absorption in the disk interior. We also need to consider that there are two surface layers; one above the midplane and the other below it. The flux from the disk interior is also treated as a monochromatic wave with $\lambda \sim 3000/T_i$ μm. Note that flux from the interior has longer wavelengths because the disk interior is cooler (see C01 for a graph for the disk interior T_i). From the two fluxes, we can calculate an anisotropic component of the radiation energy density. We use the fact that the disk surface density is given by $\Sigma = 1000 r_{\rm AU}^{-3/2}$ cm^{-2} and that the height of the disk $H(r)$ can be calculated from

$$H/r \sim 4\sqrt{T_i/T_c}\sqrt{r/R_*}, \tag{6}$$

where $T_c = 3\times10^{-24}GM_*/kR_*$ in cgs units. Here k is the Boltzmann constant.

We assume that grains are aligned when the ratio $(\omega_{\rm rad}/\omega_T)^2_{\lambda\sim a}$ exceeds 10, which is overly conservative according to a recent study in Hoang & Lazarian (2007). Figure 3 shows that at large r, large grains are aligned, even deep inside the interior. Here we take λ as the $\lambda_{\rm max,Wien}$ of the local blackbody radiation field at r. On the other hand, at small r, only grains near the disk surface are aligned, because gas density is low, and therefore, the gas drag is smaller near the surface layer. The bottom panel of Figure 3 shows that almost all grains are aligned when $r > 10$ AU. Therefore, we expect strong polarized emission from the outer part of the disk.

In the surface layer, grains are aligned by the starlight. Note that the radiation field scales as r^{-2}. Since the column density scales as $r^{-3/2}$ and the disk height is an increasing function of r, the density in the disk surface will drop faster than $r^{-3/2}$. The gas temperature in the surface layer roughly scales as $r^{1/2}$ (see CG97 and C01). Therefore, we expect that the ratio $\omega_{\rm rad}/\omega_T$ is an increasing function of r (see eq. [2]). This implies that grains at large r are aligned. Grains near the central star cannot be aligned due to high gas density near the star. Indeed, Figure 4 shows the ratio $(\omega_{\rm rad}/\omega_T)^2_{\lambda\sim a}$ exceeds 10 when $r \geq 1$ AU, which means that grains in the surface layer are aligned when $r \geq 1$ AU. Note that the radiation from the central star has a $\lambda_{\rm max,Wien}$ at $\sim$750 nm. We expect that polarized emission from the surface layer also originates from the outer part of the disk.

3. THEORETICAL ESTIMATES OF DEGREE OF POLARIZATION

In this section, we estimate the degree of polarization of emitted radiation in IR wavelengths. We need only the grain-size distribution for the calculation in this section. We do not use a detailed disk model. The discussion in this section is applicable for any system with large grains.

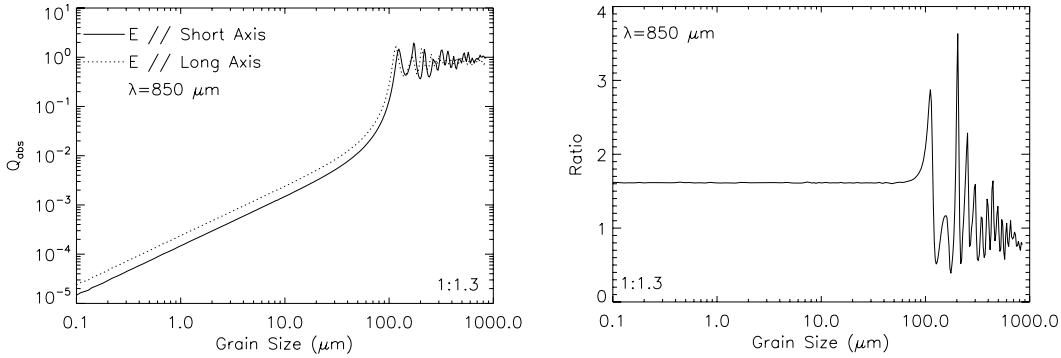

FIG. 5.—Relation between the absorption cross section (Q_{abs} times the geometric cross section) and grain size. The wavelength at which we observe is 850 μm. The grains are oblate spheroids made of silicate with the symmetry axis $\hat{\boldsymbol{a}}_1$ parallel to y-axis. The axis ratio is 1:1.3. Radiation is propagating along the x-axis. *Left*: When grains are smaller than $\sim 850/2\pi$, we can observe polarization, because the two cross sections are different. When grains are larger than $\sim 850/2\pi$, we cannot observe polarization because the two cross sections are similar. *Right*: When the axis ratio is 1:1.3, the ratio of Q_{abs} is around ~ 1.6 when the grain is small compared with the wavelength (i.e., $2\pi a/\lambda < 1$) and ~ 1 for the geometrical optics regime (i.e., $2\pi a/\lambda > 1$).

Suppose that all grains are perfectly aligned. Then, what will be the observed degree of polarization? Of course, we do not observe 100% polarization. The size parameter $2\pi a/\lambda$ plays an important role here. There are three important points that determine the degree of polarization of emitted radiation.

First, when the grain is small compared with the wavelength (i.e., when $2\pi a/\lambda < 1$), the grain's intrinsic shape gives a limit. Suppose that grains are oblate spheroids, that the symmetry axis of the grain is parallel to the y-axis, and that radiation is propagating along the x-axis. When we send two linearly polarized radiation fields with electric fields parallel to and perpendicular to the grain's symmetry axis, the radiation fields experience different cross sections; the radiation with $\boldsymbol{E} \parallel \hat{\boldsymbol{a}}_1$ sees a smaller cross section. Here $\boldsymbol{E}$ is the electric field of the radiation field and $\hat{\boldsymbol{a}}_1$ is the grain's symmetry axis. As a result, we observe polarization because the two cross sections are different. So far we have dealt with polarization by absorption. Polarization by emission is caused by exactly the same fact that the two cross sections are different. Since $Q_{abs} = Q_{em}$, where Q_{em} is the grain emissivity, a grain emits more radiation with $\boldsymbol{E} \perp \hat{\boldsymbol{a}}_1$ than one with $\boldsymbol{E} \parallel \hat{\boldsymbol{a}}_1$. The degree of polarization of emitted light is $(Q_{abs,\perp} - Q_{abs,\parallel})/(Q_{abs,\perp} + Q_{abs,\parallel})$, where $\parallel$ and $\perp$ refer to directions parallel and perpendicular to the grain's symmetry axis $\hat{\boldsymbol{a}}_1$.

Figure 5, obtained from the DDSCAT package, shows this effect clearly. The radiation fields have $\lambda = 850$ μm and the grains' long-to-short axis ratio is 1.3:1. The ratio of two cross sections is around 1.6 for $2\pi a/\lambda < 1$. When we observe emission from those grains, the degree of polarization can be as large as $(1.6 - 1)/(1.6 + 1) = 22\%$. If we assume that the grains' long-to-short axis ratio is 1.5:1, the ratio of the cross sections is 2.1:1, and the resulting degree of polarization for emission is as large as $(2.1 - 1)/(2.1 + 1) = 35\%$. The ratio of the cross sections varies as the wavelength of radiation varies. The ratio seems to be fairly constant for $\lambda > 100$ μm. However, for shorter wavelengths, the ratio decreases (Fig. 6). The shape of grains in the protostellar disk is uncertain (see, for example, Hildebrand & Dragovan [1995] for the general ISM cloud cases).

Second, when $2\pi a/\lambda > 1$ (i.e., in the geometrical optics regime), we do not observe polarization. Figure 5 clearly shows that the ratio of cross sections becomes very close to 1 when $2\pi a/\lambda > 1$. This means that the usual argument about polarization by absorption or emission works only when the grain size is small compared with the wavelength: $2\pi a/\lambda < 1$. That is, in the small-size parameter case, when radiation meets an elongated grain, it recognizes the elongated shape and interacts differently depending on the direction of the electric field of the radiation. However, in the geometrical optics regime (i.e., when $2\pi a/\lambda > 1$), radiation does not recognize that grains are elongated. We can easily understand this fact when we consider an elongated macroscopic object. Cross sections are the same regardless of the electric field directions for visible light. This second point is somewhat tricky. Even in the case in which grains are actually "aligned," we do not "observe" polarization when the grains are large compared with the wavelength.

This observation has an important consequence. When we calculate polarization, large grains (i.e., grains with $a > \lambda/2\pi$) do

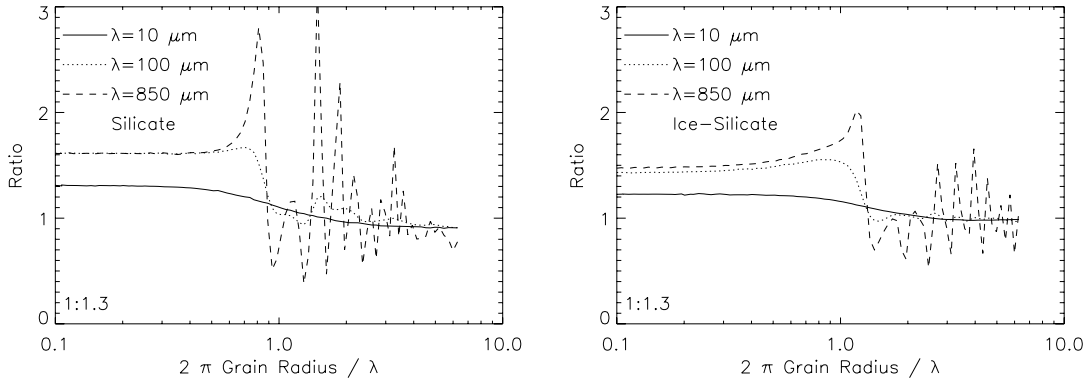

FIG. 6.—Ratio $Q_{abs,\perp}/Q_{abs,\parallel}$ vs. wavelength. *Left*: Silicate grains. For $\lambda \geq 100$ μm, the ratio is ~ 1.6 when the size parameter is less than 1 (i.e., $2\pi a/\lambda < 1$). However, for shorter wavelengths, the ratio for $2\pi a/\lambda < 1$ drops: it is ~ 1.3 for $\lambda = 10$ μm. *Right*: Ice-silicate grains (i.e., grains with silicate core and water ice mantle).

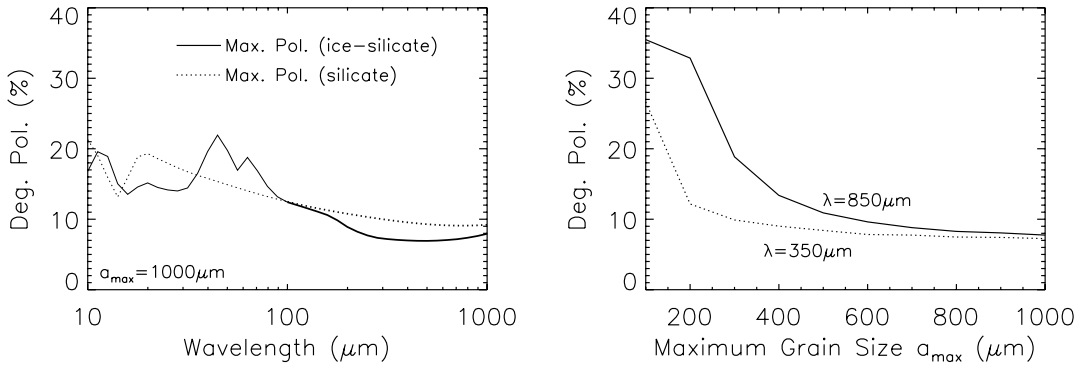

FIG. 7.—Expected maximum degree of polarization for disk interior. *Left*: $a_{\rm max} = 1000$ μm. We assume grains are oblate spheroids with an axis ratio of 1.5:1. *Right*: Degree of polarization is very sensitive to the maximum grain size $a_{\rm max}$. Results are for ice-silicate. When $a_{\rm max}$ is smaller, more grains are in the geometrical optics regime, and hence, the degree of polarization rises for a given observing wavelength.

not contribute to polarization even when they are aligned. This fact reduces the degree of polarization significantly in protostellar disks. For example, suppose that we have grains as large as 1000 μm in a disk. If we observe emission from the disk at $\lambda = 850$ μm, grains with $a > 850/2\pi \sim 100$ μm do not contribute polarization, although they dominate extinction when the grain-size distribution is a power law ($dN \propto a^{-q} da$) with $q < 3$.

Third, if the medium is optically thick, the degree of polarization reduces. The intensity of radiation from a uniform slab is $S_\nu(1 - e^{-\tau})$, where S_ν is the source function and τ is the optical depth. We can observe polarization when τ is different for parallel and perpendicular directions (to the grain symmetry axis or, generally, to any spatial direction). However, in the optically thick limit, the intensity becomes equal to S_ν. Therefore, a difference in the optical depth does not produce an observable level of polarization when the slab is opaque.

For the *disk interior*, let us consider only the first and the second points mentioned above. That is, let us assume that the grains are perfectly aligned and the disk is optically thin. We can estimate the degree of polarization p for the disk interior by integrating

$$p(\lambda) = \frac{\int_{a_{\rm min}}^{\lambda/2\pi} \left[Q_{{\rm abs},\perp}(a) - Q_{{\rm abs},\parallel}(a)\right] a^2 N(a) da}{\int_{a_{\rm min}}^{a_{\rm max}} \left[Q_{{\rm abs},\perp}(a) + Q_{{\rm abs},\parallel}(a)\right] a^2 N(a) da}, \qquad (7)$$

where the Q terms are grain absorption efficiency or grain emissivity and $a_{\rm min} = 0.01$ μm. In the left panel of Figure 7 we use $a_{\rm max} = 1000$ μm. We use $dN \propto a^{-q} da$ with $q = 3.5$ and assume that grains are oblate spheroids with a long-to-short axis ratio of 1.5:1. It is not surprising that the degree of polarization rises when we use smaller $a_{\rm max}$; when $a_{\rm max}$ is smaller, more grains are in the geometrical optics regime. The right panel of Figure 7 shows this effect.

Note that we do not use actual disk models here. Actual numerical simulations using actual disk models will give smaller values, because not all grains are aligned and some part of the disk is optically thick.

The left panel of Figure 7 shows that the maximum degree of polarization for $\lambda \leq 100$ μm is slightly larger than that for $\lambda \geq 100$ μm. However, in reality we do not expect a significant degree of polarization for $\lambda < 100$ μm, because the entire disk becomes optically thick for $\lambda < 100$ μm. The opacity per unit mass for $\lambda = 100$ μm is around $\sim O(0.1)$ (see Fig. 3 in C01). The outermost disk has column density of 1 g cm^{-2}. Therefore, even the outermost part of the disk becomes optically thick when the wavelength drops below ~ 100 μm.

For the *disk surface layer*, the second point mentioned above is irrelevant, because grains are smaller in the surface layer: $a_{\rm max} = 1$ μm. The third point is also irrelevant because the surface layer is optically thin at FIR and submillimeter wavelengths. Therefore, if all grains are perfectly aligned, the degree of polarization of the emitted radiation is determined only by the grain shapes (see the first point above).

4. ESTIMATES FOR SPECTRAL ENERGY DISTRIBUTION

In this section, we calculate the degree of polarization of emitted IR radiation from a disk with structure and parameters described in C01. In this section, we assume that the disk is face-on. The degree of polarization will be zero for a face-on disk when magnetic field is perfectly azimuthal and the disk is cylindrically symmetric. In this section, we are concerned only with the *absolute magnitude* of the polarization.

4.1. *Spectral Energy Distribution*

When $(\omega_{\rm rad}/\omega_T)^2_{\lambda\sim a}$ is larger than 10, we find the minimum aligned size from equation (5),

$$a_{\rm lower} \sim \left[\frac{10}{(\omega_{\rm rad}/\omega_T)^2_{\lambda\sim a}}\right]^{1/6} \lambda_{\rm max,Wien}, \qquad (8)$$

where $\lambda_{\rm max,Wien}$ is the peak wavelength of the aligning radiation. Grains smaller than $a_{\rm lower}$ are not aligned.

When $(\omega_{\rm rad}/\omega_T)^2_{\lambda\sim a}$ is larger than 10, we find the maximum size of grains that give rise to polarization from

$$a_{\rm upper} = \min\left(10\lambda_{\rm max,Wien},\ \lambda_{\rm obs}/2\pi\right), \qquad (9)$$

where $\lambda_{\rm obs}$ is the observing wavelength. In most cases, $a_{\rm upper} = \lambda_{\rm obs}/2\pi$, because $\lambda_{\rm max,Wien}$ falls in FIR wavelengths. Note again that the actual maximum aligned size can be larger than $a_{\rm upper}$.

Now we know $a_{\rm upper}$ and $a_{\rm lower}$. Note that $a_{\rm upper}$ and $a_{\rm lower}$ are functions of the distance to the central star r and the distance to the disk midplane z. We calculate the parallel (with respect to the local magnetic field) and perpendicular opacity, respectively,

$$\tau_\parallel(r,z) \propto \int_{a_{\rm min}}^{a_{\rm max}} Q_{\rm abs}(\pi a^2) N(a) f_\parallel \, da, \qquad (10)$$

$$\tau_\perp(r,z) \propto \int_{a_{\rm min}}^{a_{\rm max}} Q_{\rm abs}(\pi a^2) N(a) f_\perp \, da, \qquad (11)$$

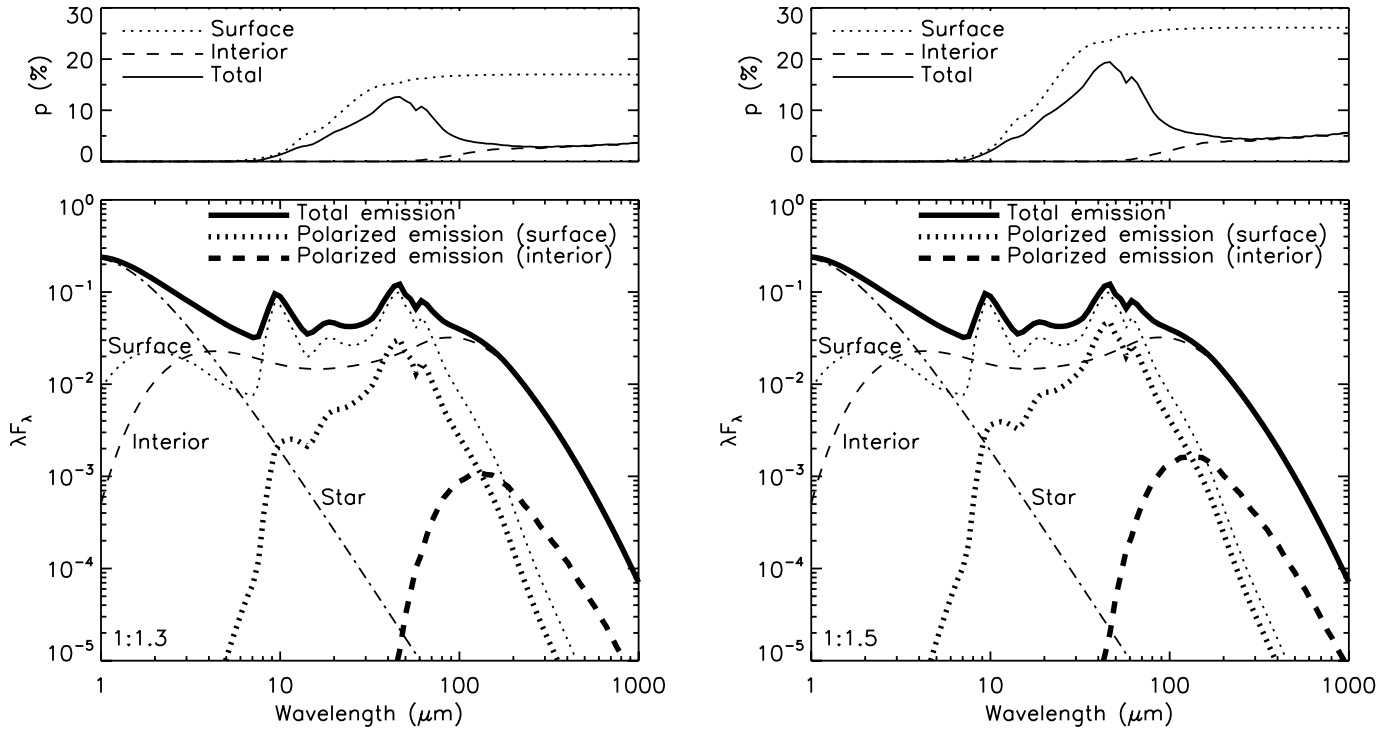

FIG. 8.—Spectral energy distribution. The vertical axis (i.e., λF_λ) is in arbitrary units. *Thick solid line*: Total (i.e., interior + surface) emission from disk. *Thin dotted line*: Total emission from disk surface. *Thick dotted line*: Polarized emission from disk surface. *Thin dashed line*: Total emission from disk interior. *Thick dashed line*: Polarized emission from disk interior. Note that in these calculations of polarized emission, we ignored the direction of polarization vectors, and we only take the absolute value of them. *Left*: Results for oblate spheroid grains with axis ratio of 1.3:1. *Right*: Results for oblate spheroid grains with axis ratio of 1.5:1. The degree of polarization is larger than that in the left panel.

where $N(a)da \propto a^{-3.5}$ (i.e., an MRN-type distribution) and

$$f_\parallel = \begin{cases} \sim 0.77 \text{ (or } \sim 0.65), & \text{if } a_{\rm lower} < a < a_{\rm upper}, \\ 1, & \text{otherwise}, \end{cases} \quad (12)$$

and

$$f_\perp = \begin{cases} \sim 1.23 \text{ (or } \sim 0.65), & \text{if } a_{\rm lower} < a < a_{\rm upper}, \\ 1, & \text{otherwise}, \end{cases} \quad (13)$$

where we assume that the long-to-short axis ratio of the oblate spheroid is 1.3:1 (or 1.5:1).

From this, we can calculate emission in parallel and perpendicular directions, respectively,

$$L_{\lambda,\parallel} \propto \lambda \int_{r_{\rm min}}^{r_{\rm max}} dr\, r \int_{-4h}^{4h} dz \frac{d\tau_{\lambda,\parallel}}{dz} e^{-\tau_\parallel} B_\lambda(T), \quad (14)$$

$$L_{\lambda,\perp} \propto \lambda \int_{r_{\rm min}}^{r_{\rm max}} dr\, r \int_{-4h}^{4h} dz \frac{d\tau_{\lambda,\perp}}{dz} e^{-\tau_\perp} B_\lambda(T), \quad (15)$$

where $\tau_\parallel$ and $\tau_\perp$ measure optical depths from z to $4h$ along the axis perpendicular to the disk midplane (see CG97). We use the BHCOAT.f and BHMIE.f codes from Bohren & Huffman (1983) to calculate grain emissivity $Q_{\rm abs}$.

The degree of polarization is

$$p(\lambda) = (L_{\lambda,\perp} - L_{\lambda,\parallel})/(L_{\lambda,\perp} + L_{\lambda,\parallel}). \quad (16)$$

Figure 8 (*left*, 1.3:1 oblate spheroid; *right*, 1.5:1 oblate spheroid) shows the results. The degree of polarization can be as large as ~5% in FIR/submillimeter wavelengths and ~ 10% in mid-IR regimes. The polarized emission at FIR is dominated by the disk interior and that at mid-IR is dominated by the disk surface layer. Note again that in these calculations, we ignored the direction of polarization, and we only take its absolute value.

4.2. *Radial Energy Distribution*

Figure 9 shows radial distribution of emitted radiation. For $\lambda = 850$ μm, both radiation from the disk interior and the surface layer are dominated by the outer part of the disk. But for $\lambda = 10$ μm, the inner part of the disk contributes a significant portion of total emission and polarized emission.

5. EFFECTS OF DISK INCLINATION

In this section we calculate actual degree of polarization that we can observe. Chiang & Goldreich (1999) calculated spectral energy distributions (SEDs) from inclined disks. We follow a similar method to calculate the SED of polarized emission. The SED of the disk interior is the integral of the source function,

$$L_\lambda^{\rm int} \propto \lambda \int_{-r_{\rm max}}^{r_{\rm max}} dx \int_{-y(x)}^{y(x)} dy \int d\tau_\lambda\, B_\lambda(T_i) e^{-\tau_\lambda}, \quad (17)$$

where

$$y(x) = \sqrt{r_{\rm max}^2 - x^2}\cos\theta - H(r_{\rm max})\sin\theta, \quad (18)$$

$r_{\rm max}$ is the outer disk radius, $H(r_{\rm max})$ is the height of disk at the disk outer radius, θ is the angle between disk symmetry axis and the line of sight, T_i is the temperature of disk interior, B_λ is the Planck function, and τ is the optical depth. The $d\tau_\lambda$ integral is

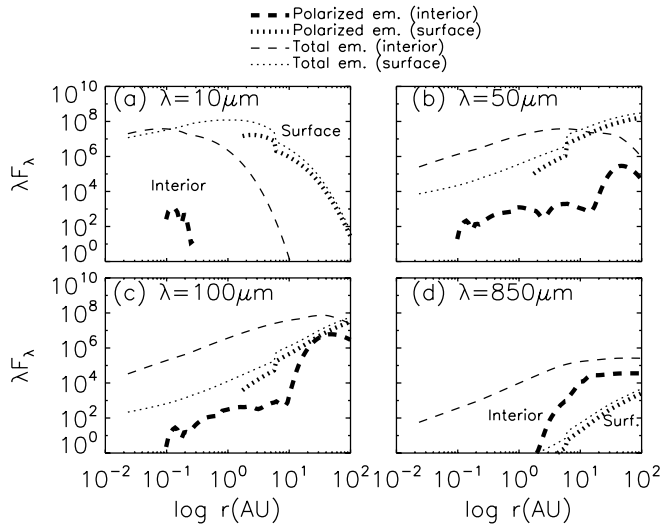

FIG. 9.—Radial energy distribution. (*a*) $\lambda = 10$ μm. Inner part of the disk emits substantial amount of radiation. But it emits negligible amount of polarized radiation. Note that when $r < 1$ AU, grains in the surface layer are not aligned and only negligible fraction of grains are aligned in the interior (see Figs. 3 and 4). (*b*) $\lambda = 50$ μm. (*c*) $\lambda = 100$ μm. (*d*) $\lambda = 850$ μm. The result for $\lambda = 450$ μm (*not shown*) is very similar to that for $\lambda = 850$ μm.

taken over the line of sight (see Chiang & Goldreich 1999 for details). The SED of the disk surface is obtained from the integral

$$L_\lambda^{\rm surf} \propto \lambda \int_{-r_{\rm max}}^{r_{\rm max}} dx \int_{-y(x)}^{y(x)} dy \sum B_\lambda(T_{ds}) \times \left[1 - \exp\left(-\frac{\alpha\epsilon_s}{|\hat{\boldsymbol{n}}\cdot\hat{\boldsymbol{l}}|}\right)\right] \exp(-\tau_\lambda), \qquad (19)$$

where $\hat{\boldsymbol{n}}$ and $\hat{\boldsymbol{l}}$ are unit vectors normal to the surface and parallel to the line of sight, respectively, ϵ_s is the Planck averaged dust emissivity at the surface. The summation is performed whenever the line of sight intersects the surface (see Chiang & Goldreich 1999 for details).

In our calculations, we explicitly take care of the fact that the grain symmetric axis is changing along a given line of sight. We follow the description in Roberge & Lazarian (1999; see also Lee & Draine 1985) to calculate this effect and we obtain optical depths with respect to the x- and y-directions in the above integrals (eqs. [17] and [19]).[3] After calculating the optical depths, we calculate $L_{\lambda,x}$ and $L_{\lambda,y}$. We obtain the luminosity for two more directions, which are at 45° with respect to x- and y-directions. We calculate the direction and degree of polarization based on the luminosity for these four directions.

Figure 10 shows the effects of the disk inclination. We calculate the polarized emission from the disk interior. The viewing angle θ (the angle of disk inclination) is the angle between the

[3] Let the z-axis be the direction of the line of sight and the y_0-axis the direction along the projection of the magnetic field on to the plane of the sky. The x_0-axis is perpendicular to both axes. Then, the cross sections C_{x0} and C_{y0} are

$$C_{x0} = C_{\rm avg} + \tfrac{1}{3}R(C_\perp - C_\parallel)(1 - 3\cos^2\zeta),$$
$$C_{y0} = C_{\rm avg} + \tfrac{1}{3}R(C_\perp - C_\parallel),$$

where $C_{\rm avg} = (2C_\perp + C_\parallel)/3$, $C_\perp$ and $C_\parallel$ are cross sections with respect to the magnetic field, and ζ is the angle between the magnetic field and the plane of the sky. We assume the Rayleigh reduction factor, R, is 1. For the x- and y-axes that also lie in the plane of the sky,

$$C_x \approx C_{x0}\cos^2\theta + C_{y0}\sin^2\theta,$$
$$C_y \approx C_{x0}\sin^2\theta + C_{y0}\cos^2\theta,$$

where θ is the angle between the x- and x_0-axis.

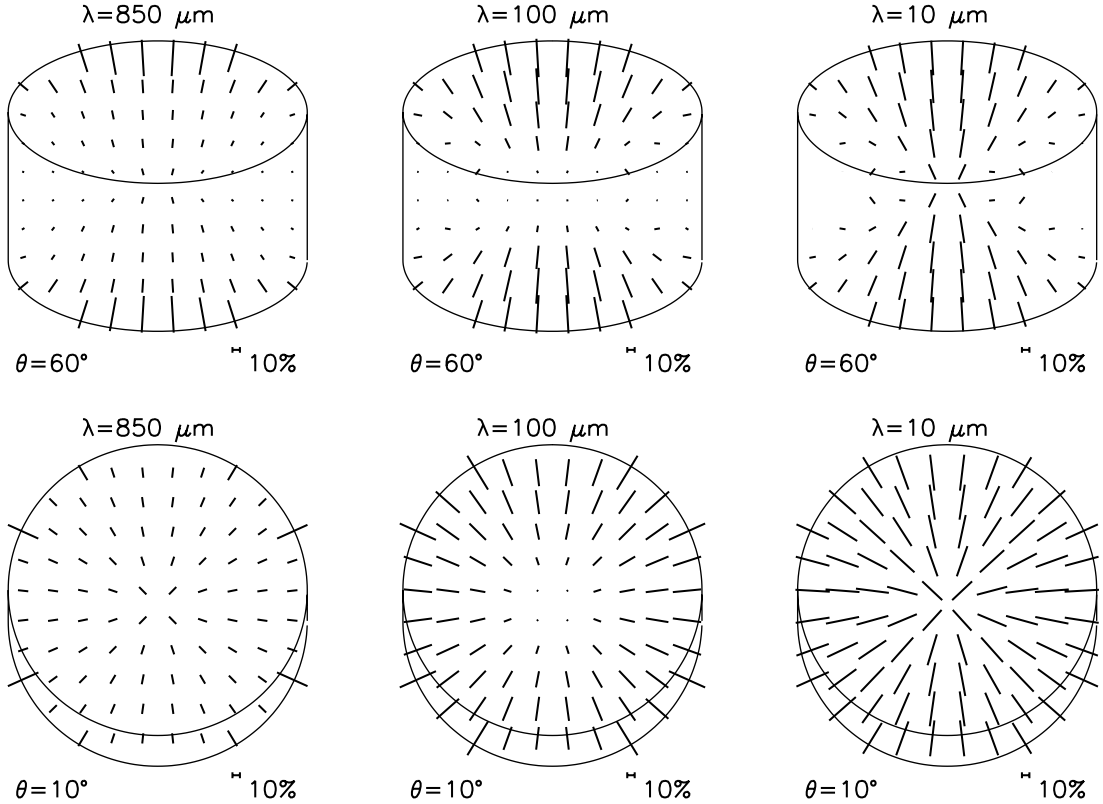

FIG. 10.—Simulated observations. Degree of polarization is calculated for the total radiation (i.e., interior + surface) from the disk. The disk inclination angle θ is the angle between disk symmetry axis and the line of sight.

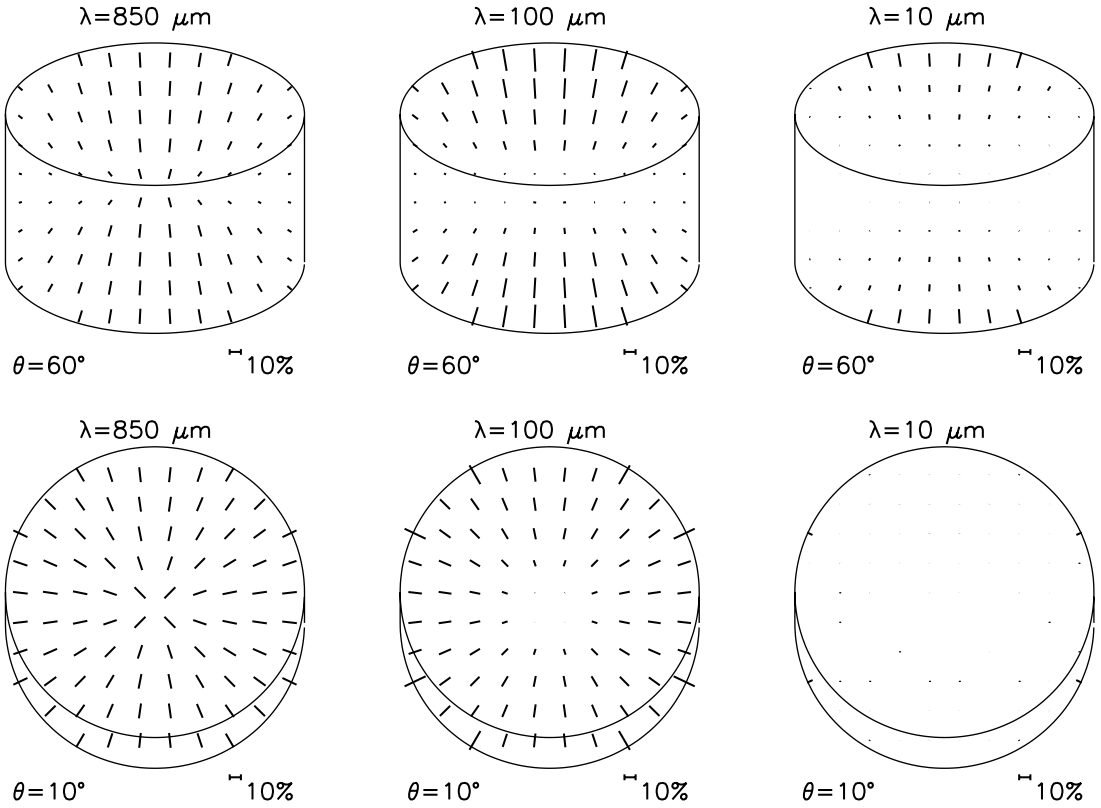

FIG. 11.—Simulated observations. Degree of polarization is calculated for the radiation from the disk interior only.

disk symmetry axis and the line of sight. We plot the direction of polarization for three different wavelengths and two different viewing angles. The lines represent the direction of polarization. Since we assume that magnetic field is azimuthal, the direction of polarization is predominantly radial (see Fig. 10, *bottom*). In Figure 11 we show similar plots for radiation from the disk interior only. For $\lambda > 100$ μm, the polarization patterns in Figure 11 are very similar to those in Figure 10. But near the disk edges, Figure 10 shows a larger degree of polarization than Figure 11, because the emission from the disk interior is very weak there compared with that from the disk surface layer. For $\lambda < 100$ μm, the polarization patterns in Figure 11 are very different from those in Figure 10, because polarized emission from the disk surface layer dominates that from the disk interior. Note that since the degree of polarization of emission from the disk surface layer is very sensitive to the maximum grain size in the surface layer, the results for $\lambda < 100$ μm should be very sensitive to the maximum grain size in the surface layer.

While the polarimetry of the spatially resolved accretion disks is promising with a new generation of instruments (see § 6.2), at present one can study disk magnetic fields with unresolved accretion disks. Below we provide predictions for this case. Figure 12 shows a SED for such a disk for four different viewing angles. When $\theta = 90$ (i.e., for edge-on disk), the inner part of the disk (i.e., region close to the star) is invisible due to high opacity. Therefore, the SED truncates for $\lambda < 10$ μm. When $\theta = 0$ (i.e., for face-on disk), the polarized emission is zero as expected.[4]

Finally, Figure 13 shows the change of the degree of polarization for selected wavelengths. The left panel shows the degree of polarization for total emission, while the right panel shows that for radiation from the interior only. The degree of polarization is large

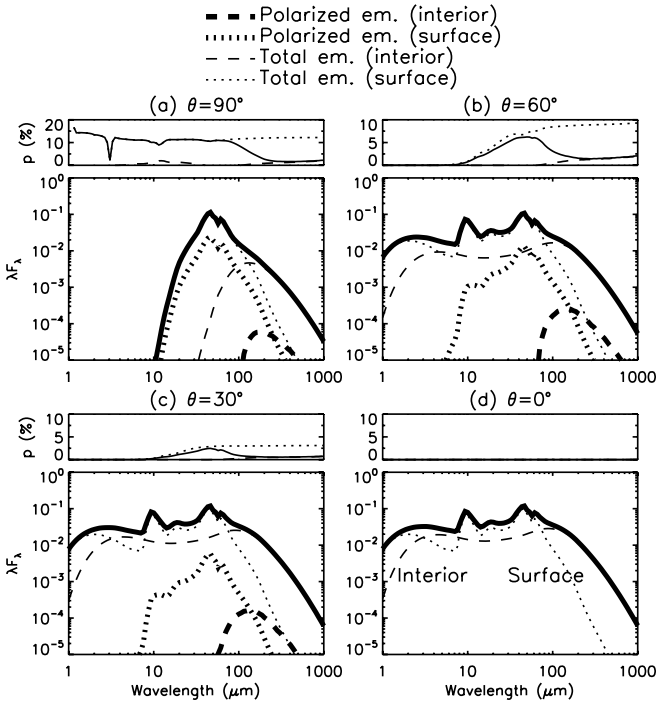

FIG. 12.— SED for four different viewing angles. When $\theta = 90$ (i.e., for edge-on disk), inner part of the disk (i.e., region close to the star) is invisible because it is occulted by the outer part of the disk. Therefore, the SED truncates for $\lambda < 10$ μm. When $\theta = 0$ (i.e., for face-on disk), the polarized emission is zero as expected, because the assumed magnetic field configuration is perfectly azimuthal.

[4] That is, we do not see thick dotted or thick dashed lines in Fig. 12*d*.

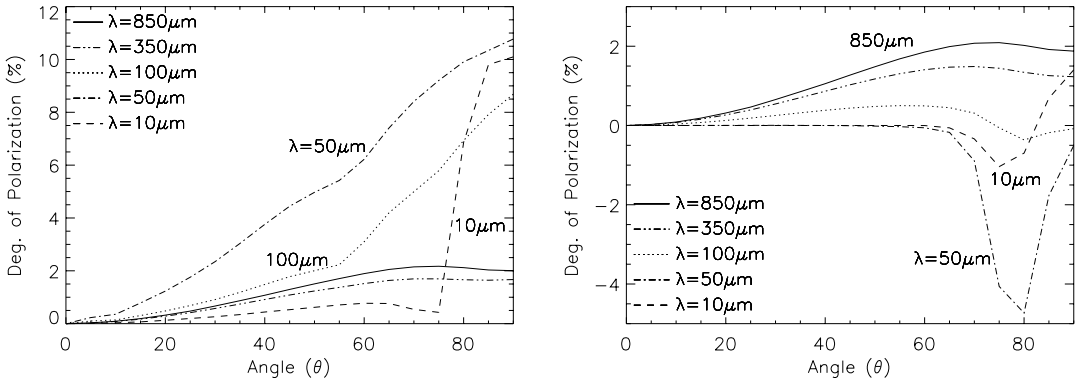

FIG. 13.—Degree of polarization vs. viewing angle. The left panel shows the degree of polarization for total (i.e., interior + surface) emission, while the right panel shows this for radiation from disk interior only.

when the angle θ is small (see Fig. 13, *left*). The sudden drop for $\lambda = 10$ μm is due to the following reason; as the viewing angle drops, the inner part of the disk suddenly becomes visible, which causes a sudden increase of the total intensity (or flux). But, the polarized intensity (or flux) does not change much, because the inner part of disk does not emit polarized emission. Note that grains are not aligned in the inner part of the disk. For $\lambda = 50$ μm, polarization is dominated by the disk surface layers.

6. DISCUSSION

6.1. *Other Alignment Processes*

In the paper above we concentrated on only one alignment process, namely, on the RT mechanism. This mechanism has became so promising in the explanation of interstellar polarization, partially because the main competitor, namely, the paramagnetic alignment mechanism (Davis & Greenstein 1951), and its later modifications were shown to have problems with aligning interstellar grains. In fact, the fast spin-up mostly due to H_2 formation on the catalytic sites over grain surface as suggested in Purcell (1979) is a textbook process that is invoked to explain the efficient paramagnetic alignment. Indeed, fast rotating grains should be immune to randomization by atomic bombardment and thus get aligned well. However, the Purcell's spin-up was shown to be inefficient for most of grains in diffuse interstellar gas due to the thermal flipping of grains that was reported in Lazarian & Draine (1999a, 1999b). The thermal flips arise from the coupling of vibrational and rotational degrees of freedom stemming from the processes of internal relaxation within interstellar grains, in particular, Barnett (Purcell 1979) and nuclear relaxation (Lazarian & Draine 1999b). As a result of flipping, the direction of the Purcell's torques acting on a grain alters and the grain gets "thermally trapped." It rotates at a thermal velocity and therefore is subjected to the randomization due to random gaseous and ionic bombardment.

The difference of the interstellar and disk grains is their size. The larger grains in the disk are not thermally trapped. Therefore, potentially the processes of Purcell's spin-up are applicable. If temperatures of grains and ambient gas are different, this may result in a spin-up that arises from variations of the accommodation coefficient over the grain surface (Purcell 1979), provided that the temperatures of the gas and the grains in the disk differ. The problem of such a scenario is that the paramagnetic alignment is slow, unless grains demonstrate enhanced magnetic susceptibility (e.g., are superparamagnetic; see Jones & Spitzer 1967). Potentially, this process that also aligns grains with long axes perpendicular to the magnetic field can enhance the alignment and therefore polarization. However, we do not know about the abundance of the required grains within the disks.

For the largest grains, a particular mechanical alignment, which was termed in Lazarian (1994) the "weathercock mechanism," is applicable. In the presence of gas-grain motions, large irregular grains would tend to get aligned with the long dimension along the flow, as their center of pressure and center of mass do not coincide. However, the mechanism requires substantial relative velocities of gas and grain, which is not certain in the protostellar disks. Moreover, we have showed above that very large grains do not produce polarized radiation at the wavelength we deal with in this paper.

More promising may be the alignment of helical grains first mentioned in Lazarian (1995) and discussed at some depth in Lazarian & Hoang (2007). The mechanism is based on the interaction of an irregular grain with a flow of atoms. If some fraction of colliding atoms is not being absorbed by the grain surface due to the grain accommodation coefficient not being equal to unity, the collisions with a flow of gaseous atoms should cause the alignment similar to that by anisotropic radiative torques. However, as it is discussed in Lazarian (2007), we do not have any compelling evidence for the operation of the mechanism in the studied astrophysical environments. On the contrary, the radiative alignment has been proven to provide the observed alignment in a number of circumstances (see Lazarian 2007). Thus, we defer a quantitative discussion of the mechanical alignment of helical grains. If the mechanism operates efficiently, it can only increase the degree of alignment at the parts of the disk where the radiative torques start to fail, making polarization from aligned grains only more important. All in all, while further studies of alternative alignment mechanisms seems necessary, at present the discussed RT mechanism provides the safest bet.

6.2. *Observational Prospects*

Multifrequency observations of protostellar disks have become a booming field recently. They have advanced substantially our knowledge of the disks and allowed theoretical expectations to be tested.

Magnetic fields are essential components of the protostellar disks. They are likely to be responsible for accretion (see Nomura 2002). Therefore, observational studies of them are essential. In this respect our paper is the first, as far as we know, to attempt to provide the expectations of the polarization arising from accretion disks that is based on the predictions of the grain alignment theory.

Our study reveals that multifrequency polarimetry is very important for the protostellar disks. The synthetic observations that we provide explicitly show that observations at wavelengths less than 100 μm mostly test magnetic fields of the skin layers, while at longer wavelengths, they test magnetic fields of the bulk of the

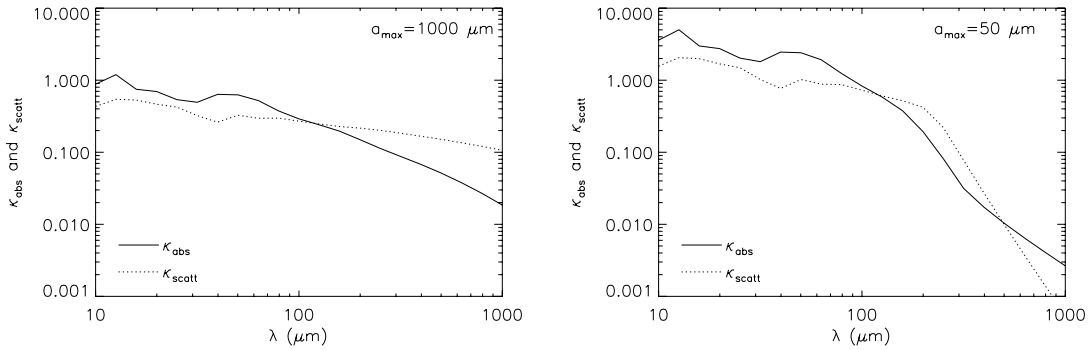

FIG. 14.—Mass absorption and scattering coefficients. The y-axes are in arbitrary units. *Left*: Maximum grain size a_{max} is 1000 μm. The scattering coefficient is larger when $\lambda > 100$ μm. *Right*: Maximum grain size a_{max} is 50 μm. The scattering coefficient is similar to or less than the absorption coefficient. In both cases, the minimum grain size is 0.01 μm.

disk. Therefore, polarimetry can, for instance, test theories of accretion, e.g., layered accretion (Gammie 1996).

Combining the FIR polarimetry with polarimetric measurements at different frequencies may provide additional insight into the magnetic properties of protostellar accretion disks. For instance, circular polarization arising from scattering of starlight from aligned grains (see Lazarian 2003) and polarization in emission lines arising from the aligned atoms (see Yan & Lazarian 2006, 2007) can provide additional information about the magnetic field in the outer parts and above the accretions disks.

Most of the present-day polarimetry will be done for unresolved protostellar disks. The size of the T Tauri disks is usually less than ~300 AU (see, for example, C01). If we take the distance to protostars to be around $\geq$100 pc, then the angular sizes of the disks are usually smaller than 6″. The angular resolution of the SCUBA polarimeter (SCUPOL) is around 14″ (Greaves et al. 2000) and that of the SHARC II polarimeter (SHARP; Novak et al. 2004) at 350 μm is around 9″. Therefore, it is not easy to obtain plots like Figure 10. The angular resolution of the intended SOFIA polarimeter is around 5″ at 53 μm, 9″ at 88 μm, and 22″ at 215 μm. We see that the intended SOFIA polarimeter will be at the edge of resolving the structure of close-by disks, while other instruments will not resolve a typical T Tauri disk. Therefore, for most of the near-future observations, our predictions in Figures 13 and 14 are most relevant.

Higher resolution polarimetry is expected in future, however. This will make our predictions of polarization in the resolved accretion disks in Figures 11 and 12 testable. Note that the actual structure of magnetic fields may be much more complex than that in our simple model.

While in this paper we dealt with the protostellar accretion disks, our results are suggestive of the importance of polarimetric studies of magnetic fields in the disks of evolved stars. In a broader context, the present paper is one of the first studies to make use of the advances in grain alignment theory to extend the utility of polarimetric studies of magnetic fields beyond its traditional interstellar domain.

6.3. *Effects of Scattering*

In this paper, we do not consider the effects of scattering. Below we show that the effects of scattering are indeed less important for emissions from disk interior in the FIR regime. We will provide more detailed calculations on the effects of scattering for shorter wavelengths elsewhere.

In the case $2\pi a/\lambda \ll 1$, we can assume that Q_{scatt} is negligibly smaller than Q_{abs}. However, since we are dealing with large grains here, we cannot simply assume the inequality. We first compare the relative magnitudes of mass scattering and absorption coefficients, κ_{scatt} and κ_{abs}, when grain-size distribution follows an MRN-type power law, $dN \propto a^{-3.5}da$, between $a_{min} = 0.01$ μm and a_{max} (see also § 2.1). Figure 14 shows that κ_{scatt} is larger than κ_{abs} for $\lambda \geq 100$ μm in the case in which $a_{max} = 1000$ μm, because the scattering efficiency is larger than that of the absorption when $\lambda \sim 2\pi a$ (Fig. 15). This trend is generally observed when

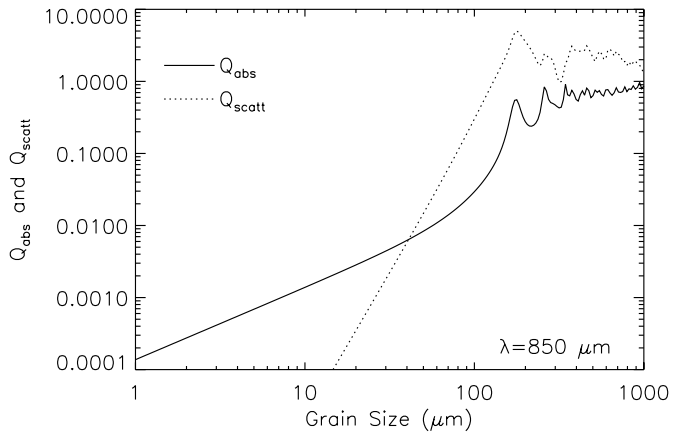

FIG. 15.—Scattering and absorption coefficients. The wavelength is fixed for $\lambda = 850$ μm. The grains are spherical silicate coated with water ice. The scattering coefficient is larger than the absorption one for large grains.

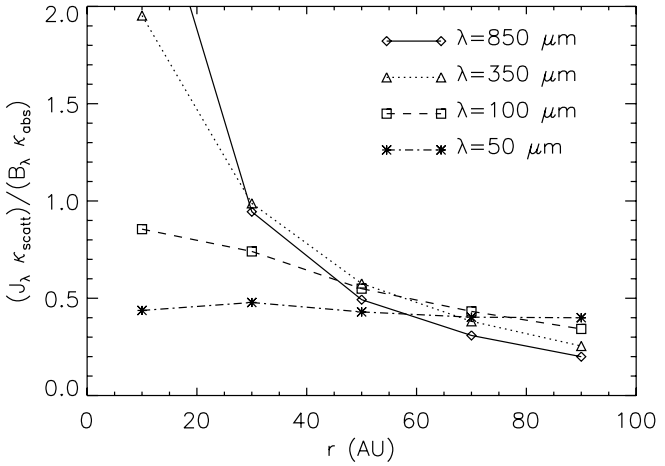

FIG. 16.—Comparison between polarization by scattering and emission. When the value in y-axis is less than 1, we expect that absorption is more important for polarization. The values are calculated in the midplane of the disk. When we calculate the values at locations above the midplane the values may be smaller.

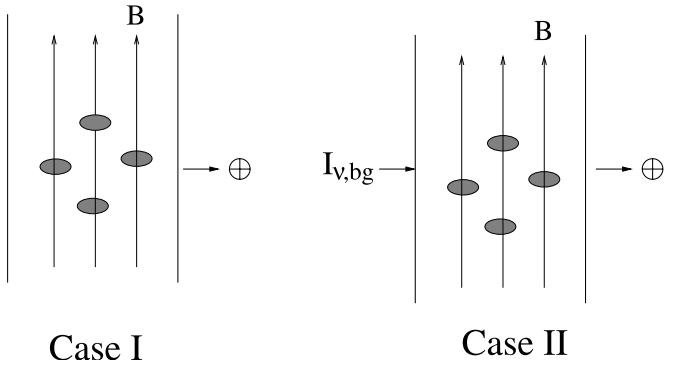

FIG. 17.—In case I, all parts of the disk along the line of sight have aligned grains. In this case, the direction of polarization is perpendicular to the magnetic field. In case II, the aligned part lies in front of the unaligned part. In this case, the direction of polarization depends on the relative strength of the local source function and the background radiation. Note that $I_{\nu,bg}$ is unpolarized radiation from background regions of the disk.

$\lambda \geq 100\ \mu$m. When the cutoff size a_{max} gets smaller, κ_{scatt} becomes subdominant (see Fig. 14, *right*).

Polarization by scattering is proportional to $\sim J_\lambda \kappa_{scatt}$, where J_λ is the mean radiation field, while polarization by emission is proportional to $\sim B_\lambda \kappa_{abs}$, where B_λ is the intensity of the blackbody radiation at the point of interest. Figure 16 shows this $J\kappa_{scatt}$-to-$B\kappa_{abs}$ ratio at selected points on the disk midplane. We use the disk model in C01 to calculate J_λ and B_λ. We only include emission from the disk interior. Recall that most FIR emission from the disk interior is from $r > 10$ AU (see Fig. 9). Therefore, the $J\kappa_{scatt}$-to-$B\kappa_{abs}$ ratio for $r > 10$ AU concerns us most. This crude estimate tells us that polarization by scattering is less important than that by emission in the FIR regime. Nevertheless, readers should keep in mind that our polarization calculations in this paper reflect only the emitted component and, therefore, the radiative transfer adopted is approximate.

How important is the self-scattering effect? Let us first consider the case in which the entire disk volume has aligned grains (Case I in Fig. 17). As we see below, self-scattering/absorption does not change the direction of polarization in case I in Figure 17. The observed radiation parallel to the magnetic field becomes

$$\begin{aligned} I_{\lambda,\parallel} &= \int B_\lambda \exp\left(-\tau_{ext,\parallel}\right) d\tau_{abs,\parallel} \\ &= \frac{1}{1+\alpha_\parallel} \int B_\lambda \exp\left(-\tau_{ext,\parallel}\right) d\left(-\tau_{ext,\parallel}\right) \\ &= \frac{B_\lambda}{1+\alpha_\parallel}\left[1 - \exp\left(-\tau_{ext,\parallel}\right)\right], \end{aligned} \tag{20}$$

where $\tau_{ext,\parallel} \equiv \tau_{abs,\parallel} + \tau_{scatt,\parallel}$, and we assume that the gas is uniform and that $\alpha_\parallel \equiv \tau_{scatt,\parallel}/\tau_{abs,\parallel}$ does not change along the line of sight. For simplicity, we ignore the radiation that scatters into the line of sight. We have a similar expression for the perpendicular direction,

$$I_\perp - I_\parallel \propto \frac{1 - \exp\left(-\tau_{ext,\perp}\right)}{1+\alpha_\perp} - \frac{1 - \exp\left(-\tau_{ext,\parallel}\right)}{1+\alpha_\parallel}, \tag{21}$$

which is positive when $\tau_{ext,\perp} > \tau_{ext,\parallel}$ and $\alpha_\perp \approx \alpha_\parallel$. This means that the direction of polarization is perpendicular to the magnetic field. Recall that most of the outer part of the disk (i.e., $r > 10$ AU) has aligned grains (see Fig. 3). Therefore, the situation is similar to case I, and we expect that including self-scattering does not change our qualitative results in earlier sections.

In case II, however, self-scattering can be potentially important. Case II will happen when we have a slab of aligned grains in front of unaligned grains (see Fig. 17). The observed intensity becomes

$$I_{\lambda,\parallel} = I_{\lambda,bg} \exp\left(-\tau_{ext,\parallel}\right) + \frac{B_\lambda}{1+\alpha_\parallel}\left[1 - \exp\left(-\tau_{ext,\parallel}\right)\right] \tag{22}$$

for the direction parallel to the magnetic field and

$$I_{\lambda,\perp} = I_{\lambda,bg} \exp\left(-\tau_{ext,\perp}\right) + \frac{B_\lambda}{1+\alpha_\perp}\left[1 - \exp\left(-\tau_{ext,\perp}\right)\right] \tag{23}$$

for the direction perpendicular to the magnetic field. Here, for simplicity, we assume the medium is uniform. In the optically thin case, we have

$$\begin{aligned} I_{\lambda,\parallel} &= I_{\lambda,bg} - I_{\lambda,bg}\tau_{ext,\parallel} + \frac{B_\lambda}{1+\alpha_\parallel}\tau_{ext,\parallel} \\ &= I_{\lambda,bg} - I_{\lambda,bg}\tau_{ext,\parallel} + B_\lambda \tau_{abs,\parallel} \end{aligned} \tag{24}$$

for the direction parallel to the magnetic field and

$$\begin{aligned} I_{\lambda,\perp} &= I_{\lambda,bg} - I_{\lambda,bg}\tau_{ext,\perp} + \frac{B_\lambda}{1+\alpha_\perp}\tau_{ext,\perp} \\ &= I_{\lambda,bg} - I_{\lambda,bg}\tau_{ext,\perp} + B_\lambda \tau_{abs,\perp} \end{aligned} \tag{25}$$

for the direction perpendicular to the magnetic field. Then we have

$$\begin{aligned} I_\perp - I_\parallel &\propto B_\lambda\left(\tau_{abs,\perp} - \tau_{abs,\parallel}\right) - I_{\lambda,bg}\left(\tau_{ext,\perp} - \tau_{ext,\parallel}\right) \\ &= \left[B_\lambda - I_{\lambda,bg}\left(1 + \frac{\tau_{scatt,\perp} - \tau_{scatt,\parallel}}{\tau_{abs,\perp} - \tau_{abs,\parallel}}\right)\right]\left(\tau_{abs,\perp} - \tau_{abs,\parallel}\right). \end{aligned} \tag{26}$$

Therefore, the direction of polarization can change as a result of scattering.

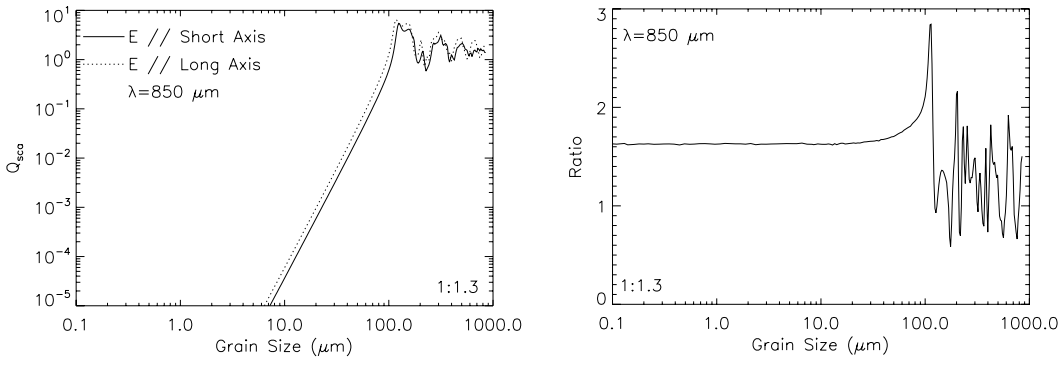

FIG. 18.—Scattering efficiency vs. grain size. When grains are oblate spheroids, the scattering cross section depends on the direction of polarization. The ratio of the scattering cross sections is very similar to that of absorption (see Fig. 5). See the caption of Fig. 5 for details.

The ratio $(\tau_{\rm scatt,\perp} - \tau_{\rm scatt,\parallel})/(\tau_{\rm abs,\perp} - \tau_{\rm abs,\parallel})$ cannot be very large. Figure 18 implies that scattering does not cause polarization in the geometrical optics regime (i.e., $\lambda/2\pi < a$). On the other hand, Figure 15 shows that scattering is negligible when a is a few times smaller than $(\lambda/2\pi)$. This means that scattering dominates polarization only for a limited range, $\beta(\lambda/2\pi) < a < (\lambda/2\pi)$, where $\beta \approx 0.2-0.3$. However, scattering dominates absorption for $\beta(\lambda/2\pi) < a$ (see Fig. 15). Therefore, we expect that (see Fig. 14 for the ratio $\kappa_{\rm scatt}/\kappa_{\rm abs}$)

$$\frac{\tau_{\rm scatt,\perp} - \tau_{\rm scatt,\parallel}}{\tau_{\rm abs,\perp} - \tau_{\rm abs,\parallel}} < \frac{\tau_{\rm scatt}}{\tau_{\rm abs}}. \quad (27)$$

7. SUMMARY

Making use of the recent advances in grain alignment theory, we calculated grain alignment by RTs in a magnetized T Tauri disk. Based on this, we calculated polarized emission from the disk. Our results show the following.

1. Polarization arising from aligned grains reveals the magnetic field of the T Tauri disk.

2. Grain-size distribution is the most important factor in determining the degree of polarization.

3. The disk interior dominates polarized emission in FIR/submillimeter wavelengths. When there are many grains with a maximum grain size of $\sim$1000 μm, the degree of polarization is around or less than $\sim$2% in these wavelengths. However, when the maximum grains are smaller, we expect a higher degree of polarization.

4. The disk surface layer dominates polarized emission in mid-IR wavelengths. The degree of polarization is very sensitive to the maximum size of grain in the disk surface layer. When the maximum grain size is as large as $\sim$1 μm, we expect $\sim$10% of polarization at $\lambda \sim 50$ μm. However, when the maximum size is smaller then the value will drop.

5. Our study of the effect of the disk inclination predicts substantial changes of the degree of polarization with the viewing angle. The coming mid-IR/FIR polarimeters are very promising for studies of magnetic fields in protostellar disks.

Jungyeon Cho's work was supported by the Korea Research Foundation grant funded by the Korean Government (KRF-2006-331-C00136). A. Lazarian acknowledges the support from the NSF grants AST 02-43156 and AST 05-07164 as well as from the NSF Center for Magnetic Self-Organization in Laboratory and Astrophysical Plasmas. The work of Jungyeon Cho was also supported in part by the Korea Foundation for International Cooperation of Science and Technology (KICOS) through the Cavendish-KAIST Research Cooperation Center.

REFERENCES

Aitken, K., Efstathiou, A., McCall, A., & Hough, J. 2002, MNRAS, 329, 647
Balbus, S. A., & Hawley, J. F. 1991, ApJ, 376, 214
Bethell, T., Chepurnov, A., Lazarian, A., & Kim, J. 2007, ApJ, 663, 1055
Bohren, C. F., & Huffman, D. R. 1983, Absorption and Scattering of Light by Small Particles (New York: Wiley)
Chandrasekhar, C. 1961, Hydrodynamic and Hydromagnetic Stability (Oxford: Oxford Univ. Press)
Chiang, E., Joung, M., Creech-Eakman, M., Qi, C., Kessler, J., Blake, G., & van Dishoek, E. 2001, ApJ, 547, 1077 (C01)
Chiang, E., & Goldreich, P. 1997, ApJ, 490, 368 (CG97)
———. 1999, ApJ, 519, 279
Cho, J., & Lazarian, A. 2005, ApJ, 631, 361 (CL05)
Davis, L., Jr., & Greenstein, J. L. 1951, ApJ, 114, 206
Dolginov, A. Z. 1972, Ap&SS, 18, 337
Dolginov, A. Z., & Mytrophanov, I. G. 1976, Ap&SS, 43, 291
Draine, B. 1985, ApJS, 57, 587
Draine, B., & Flatau, P. 1994, J. Opt. Soc. Am. A, 11, 1491
———. 2004, preprint (astro-ph/0409262)
Draine, B., & Lazarian, A. 1998, ApJ, 508, 157
Draine, B., & Lee, H. 1984, ApJ, 285, 89
Draine, B., & Weingartner, J. 1996, ApJ, 470, 551 (DW96)
———. 1997, ApJ, 480, 633
Gammie, C. 1996, ApJ, 462, 725
Greaves, J., Holland, W., Jenness, T., & Hawarden, T. 2000, Nature, 404, 732
Greenberg, M. 1968, in Nebulae and Interstellar Matter, ed. B. M. Middlehurst & L. H. Aller (Chicago: Univ. Chicago Press), 221
Hall, J. 1949, Science, 109, 166
Hildebrand, R., & Dragovan, M. 1995, ApJ, 450, 663
Hiltner, W. 1949, Science, 109, 165
Hoang, T., & Lazarian, A. 2007, ApJ, submitted
Jones, R. V., & Spitzer, L., Jr. 1967, ApJ, 147, 943
Laor, A., & Draine, B. 1993, ApJ, 402, 441
Lazarian, A. 1994, Ap&SS, 216, 235
———. 1995, MNRAS, 277, 1235
———. 2003, J. Quant. Spectrosc. Radiat. Transfer, 79, 881
———. 2007, J. Quant. Spectrosc. Radiat. Transfer, 106, 225
Lazarian, A., & Draine, B. 1999a, ApJ, 516, L37
———. 1999b, ApJ, 520, L67
Lazarian, A., & Hoang, T. 2007, MNRAS, 378, 910
Lee, H., & Draine, B. 1985, ApJ, 290, 211
Mathis, J., Rumpl, W., & Nordsieck, K. 1977, ApJ, 217, 425
Nomura, H. 2002, ApJ, 567, 587
Novak, G., et al. 2004, Proc. SPIE, 5498, 278
Purcell, E. 1979, ApJ, 231, 404
Roberge, W., & Lazarian, A. 1999, MNRAS, 305, 615
Tamura, M., Hough, J., Greaves, J., Morino, J.-I., Chrysostomou, A., Holland, W., & Momose, M. 1999, ApJ, 525, 832
Velikov, S. 1959, J. Exp. Theor. Phys., 36, 1398
Weingartner, J., & Draine, B. 2001, ApJ, 548, 296
———. 2003, ApJ, 589, 289
Yan, H., & Lazarian, A. 2006, ApJ, 653, 1292
———. 2007, ApJ, 657, 618